ATS-Note-2012-014 TECH

January 27, 2012

mariusz.sapinski@cern.ch

Estimation of Threshold for the Signals of the BLMs around the LHC Final Focus Triplet Magnets

F. Cerutti / EN-STI, B. Dehning / BE-BI, A. Ferrari / EN-STI, C. Hoa, M. Mauri, A. Mereghetti / EN-STI, M. Sapinski / BE-BI, E. Wildner / BE-ABP

Keywords: insertion region, quench prevention

Summary

The Interaction Points of the Large Hadron Collider are the regions where the two circulating beams collide. Hence, the magnets the closest to any Interaction Point are exposed to an elevated radiation field due to the collision debris. In this study the signal in the Beam Loss Monitors due to the debris is estimated. In addition, for three different scenarios of beam losses, the energy density in the coils and the signal in the Beam Loss Monitors at quench are computed. It is shown that the Beam Loss Monitors, as presently installed on the vacuum vessel of the magnets, cannot disentangle the signal due to a localised loss from the constant signal due to the debris in case of steady-state losses.

1 Introduction

The *inner triplet* [1] is a string of three superconducting quadrupoles (Q1-Q3) installed on both sides of every Interaction Point (IP) of the Large Hadron Collider (LHC), aimed at the final squeeze of the beams before collision. Due to its proximity to the IP and its strong magnetic field, the *inner triplet* is particularly exposed to the proton-proton collision debris and the risk of quench (i.e. a sudden transition from superconducting to normal conducting state) is consequently higher than for other magnets. Therefore, the impact of the debris has been carefully investigated and suitable protection solutions have been implemented [2]. Nevertheless, abnormal beam losses might occur.

In order to identify possible losses that may lead the magnets to quench, Beam Loss Monitors (BLMs) [3] are installed all along the LHC ring in order to detect an abnormal increase of the radiation field around the accelerator: if the measurements are above a predefined threshold, a beam dump signal is triggered. BLMs are nitrogen-filled ionization chambers in form of tubes about 50 cm long and with diameter of almost 10 cm [4]: eighteen of them are installed on the surface of the vacuum vessels of the *inner triplet* or in its vicinity.

Thresholds for BLMs are set for twelve signal integration times between 40 μs and 84 s as

well as for various beam energies. This study is meant to investigate thresholds for the two extreme cases of fast transient and steady state losses at the beam energy of 7 TeV. The method used for scaling these thresholds to intermediate time ranges is described in [5].

The simulations are performed with the FLUKA Monte Carlo code [6, 7]. The energy deposited in the superconducting coils ($\mathcal{E}$) and in the BLMs active gas (E_{BLM}) is scored: the relation between these two quantities represents a valuable input for setting the BLM thresholds. However, the systematic uncertainties affecting the calculation should not be neglected (in particular, "minor" geometry details not yet implemented at the stage of this work can appreciably alter E_{BLM}). Nonetheless, our conclusions concerning the possibility of detecting local abnormal losses are expected to hold.

2 Simulation Set Up

All main components of the LHC Insertion Region (IR) up to about 280 m on the right side of IP1 (ATLAS experiment) have been implemented with a detailed description of their geometry, materials and magnetic fields. The LHC tunnel and the ATLAS cavern have been modelled as well [8, 9]. A zoom on the *inner triplet* as implemented in FLUKA is shown in Figure 1.

The coils are the quench-sensitive parts of the magnets, and they are arranged in layers immediately around the beam pipe. The innermost layer is normally subject to the highest energy deposition and, due to the magnetic field strength and its large distance to the heat exchanger, has also the lowest quench margin. The energy deposited in the coils is scored in a 3D mesh, the binning of which is set according to the duration of the considered loss type (see Sections 5 and 6).

The first BLM is installed vertically in the gap between the Target Absorber of Secondaries (TAS) and Q1, only 18 cm away from the beam pipe, below the beam level; all other monitors are installed at the beam height, horizontally oriented, on the surface of the vacuum vessel, except for the last monitor, which is installed close to the beam pipe (see Figure 1). A detailed FLUKA model of the BLM including gas, electrodes, chamber walls and electronic compartment material is used [10].

The transport cut-offs used in the simulations are:

- 10^{-5} eV for neutrons;
- 1 MeV for electrons and positrons;
- 100 keV for the other particles.

The coordinate system is right-handed; the x-axis is horizontal, perpendicular to the triplet axis, pointing outside the ring; the y-axis is vertical, upwards oriented; the z-axis is oriented accordingly. The origin is in the center of the ATLAS detector, where collisions take place. On the right side of IP1, Beam 1 (B1) exits from the IP and Beam 2 (B2) moves towards the IP. The distance from IP1 measured in the direction of B1 (clockwise) is also referred to as *dcum* (from the French expression *Distance CUMulée*).

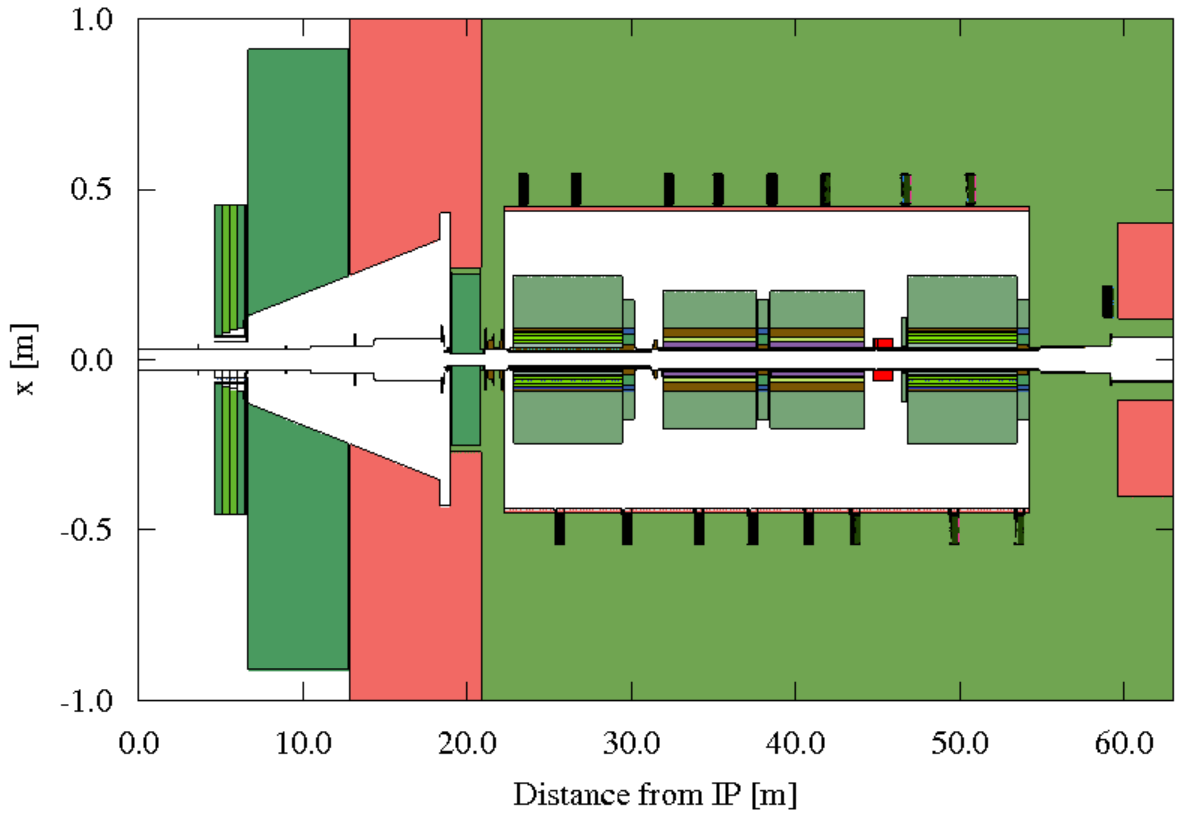

Figure 1: *Horizontal cut at beam height of the* FLUKA *geometry of IP1, right side; zoom on the inner triplet. The first monitor is not visible since it is at a different height. Note that the scale of the two axes is different.*

3 Units

The following units are used in this report:

- FLUKA provides results of energy density in the coil in GeV/cm^3 per primary event, and of energy deposited in the BLM active volume in GeV per primary event; a primary event is either a single proton-proton collision in IP1 or the loss of a single proton;
- the Quench Margin is usually expressed in mJ/cm^3 in case of fast transient losses and in mW/cm^3 in case of steady state losses;
- the BLM thresholds are given in Grays [Gy] or Grays per second [Gy/s].

4 Simulated Cases

Two main scenarios leading to energy deposition in the coils of the magnets of the *inner triplet* have been simulated: the debris from the IP and the direct beam losses. Debris is constantly present during LHC physics runs, as a result of proton-proton collisions (ion operation is not considered here); on the contrary, beam losses are unwanted phenomena which might occur due to beam missteering, optics problems or wrong settings of the collimators.

Other scenarios of dynamic load on superconducting coils are expected to have a limited impact [11]: particle showers generated in the tertiary collimators (TCTs) protecting the *inner triplet* or by the interaction of the beam with the residual gas, are predicted to induce a peak energy deposition at least two orders of magnitude lower than the one due to the debris at nominal luminosity.

4.1 Proton-Proton Collision Debris

DPMJET III [12] is the event generator used to simulate proton-proton collisions at 14 TeV center-of-mass energy, directly called from inside FLUKA. The results of the simulations are scaled by a collision rate of $8{\cdot}10^8$ s^{-1}, obtained multiplying the nominal peak luminosity $L_0 = 10^{34}$ $cm^{-2}s^{-1}$ by the proton-proton reaction cross section $\sigma = 80$ mbarn. This value of cross section includes inelastic and diffractive events. The plane of crossing of the beams is vertical and the simulated statistics is about 10^5 primary events.

4.2 Beam Losses

Three beam loss scenarios have been studied: horizontal and vertical losses on the TAS, and direct losses on the magnets of the *inner triplet* due to erroneous setting of the collimators.

4.2.1 Losses on the TAS

Despite its small aperture (34 mm diameter), the TAS, placed on the IP side of the *inner triplet*, is not a bottleneck for the beams, thanks to the small values of the optical β functions at its location. Nevertheless, a loss of the beam exiting the IP in the TAS can be of concern for the *inner triplet*, because the generated shower may propagate in the vacuum chamber and be deflected by the intense magnetic field onto the superconducting cables.

The source particles considered in these scenarios are 7 TeV protons coming from the IP and impacting the TAS at the end of its vacuum chamber, where the β function has the highest local value and the shower is only marginally absorbed by the TAS itself. An angle of 240 μrad with respect to the z-axis is assumed. The parameters for horizontal (*TAS-H*) and vertical (*TAS-V*) losses are reported in Table 1. The acquired statistics is of 10^5 primary protons.

beam-loss scenarios	*TAS-H*	*TAS-V*
impact plane	horizontal	vertical
impact point x (cm)	1.7	0
impact point y (cm)	0	1.7
impact point z (cm)	2105.0	2105.0

Table 1: *Beam parameters for the two scenarios of beam losses on the TAS.*

4.2.2 Beam Losses due to Wrong Settings of the Collimators

Simulations performed with tracking codes have widely demonstrated that the *inner triplet* is well protected against losses if the collimation system is correctly set up. On the other hand, a wrong setting of primary and secondary collimators in the LHC section dedicated to betatron cleaning (IR7) could imply losses peaked almost at the centre of Q2B [13]. A similar tracking simulation result has been obtained in case the TCTs are accidentally retracted [14].

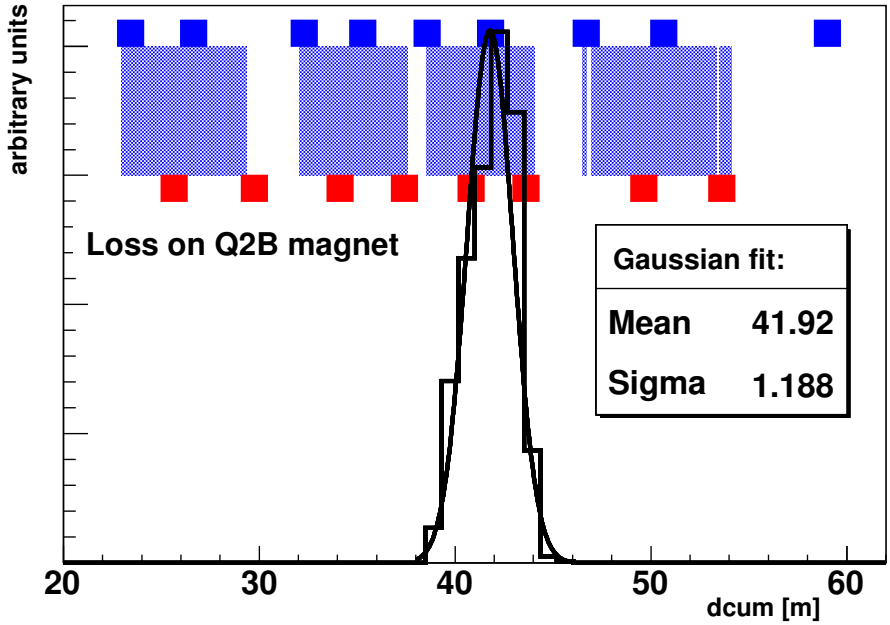

Figure 2: *Longitudinal distribution of losses for the Q2B scenario. The concerned beam (B2) comes from the right.*

Primary protons for this scenario (*Q2B*) are sampled from an analytical distribution derived from the loss maps generated with the tracking code [14], defined as follows:

- x position: -2.519 cm, i.e. inside the vacuum chamber, 10 μm away from the beam screen, on the internal side with respect to the LHC ring;
- y position: flat distribution over the interval -0.8 cm $<$ y $<$ 0.4 cm;
- z position: Gaussian distribution centered at 41.92 m from the IP (i.e. 3.43 m after the beginning of Q2B), with $\sigma = 1.1875$ m, as shown in Figure 2;
- dx/dz direction: -500 μrad (half of the times) or -875 μrad[1];
- dy/dz direction: in case of x$\prime$ $=$ -500 μrad a flat $y\prime$ distribution over the interval -200 μrad $<$ y$\prime$ $<$ 300 μrad was taken, in case of x$\prime$ $=$ -875 μrad the flat $y\prime$ distribution spanned the interval -300 μrad $<$ y$\prime$ $<$ 500 μrad.

In total 10^5 protons have been generated also for this scenario.

5 Quench Limits

The quench limit of a superconducting material depends on the current density, the actual temperature at which it operates and the intensity of the magnetic field inside the material. In case of a superconducting magnet with a given geometry of the cables, the intensity of the magnetic field and the corresponding current are set on the basis of the beam energy, and during normal operation the cryogenic system keeps the temperature constant. In case of a sudden energy deposition, a certain amount of time is needed by the heat capacity of the cooling bath

[1]A negative value means that particles are moving towards the beam screen. The values of the impacting angle are large with respect to typical losses in the arc.

and the cryogenic system to evacuate the heat. Thus, the quench limit for a superconducting magnet depends on the beam energy, the loss duration, as well as the actual distribution of deposited heat.

Only the beam energy of 7 TeV for two extreme cases of loss duration are considered for this study:

- fast transient losses: the quench limit is calculated as enthalpy limit ΔH of a dry cable (NbTi alloy and Copper). This approximation is valid only for very short loss durations, below 100 μs, for which the heat has no time to leak to super-fluid helium, featured by a large heat capacity and a very good heat conductivity. The value considered in the present study was calculated with ROXIE [15] and is[2] $\Delta\mathrm{H} = 1.2$ mJ/cm^3 $=$ $7.5 \cdot 10^6$ GeV/cm^3.

- steady-state losses: the heat has time to spread all over the cable and reach the helium bath. The quench limit is derived from the cooling power of the system by measurement [16] or by calculation [17, 18]. Advanced techniques to calculate heat flow rate take into account the energy density distribution in all coil elements [19, 20]. The value used here is[3] $\mathcal{P}_{\mathrm{QL}} = 12$ mW/cm^3 $= 7.5 \cdot 10^7$ GeV/(cm$^3 \cdot$ s).

For transient losses longer than 100 μs the algorithm described in [5] is used. Alternative solutions to estimate the quench limit for long transient losses based on heat transport codes exist [21].

6 Energy Deposition in the Superconducting Coils

The energy density distribution in the superconducting coils has been estimated with a scoring mesh in cylindrical coordinates (r, ϕ and z), normalised to one impacting proton or one proton-proton collision. Its binning has been set according to the different mechanisms ruling the quench limit:

- energy deposition due to steady state losses, $\mathcal{E}_{cable}$: since the heat has time to locally spread, the binning is sized on the volume of cable that can be considered in thermal equilibrium. This volume was assumed to be defined by the cable transverse dimensions and a longitudinal length equal to the cable transposition pitch;

- energy deposition due to fast transient losses, $\mathcal{E}$: the energy density is scored with a finer binning on the radial dimension (a step of about 2 mm has been adopted).

The highest (hereafter, "maximum") energy density value in the coils, usually correspoding to the innermost layer, determine the quench location and the number of lost protons or the loss rate needed to quench.

The patterns of $\mathcal{E}_{cable}$ produced by the debris have been described in detail in [8] and [23]. Figure 3 shows the longitudinal distribution of peak($\mathcal{E}$) and peak($\mathcal{E}_{cable}$) (both over r and ϕ) along the coils of the *inner triplet* quadrupoles. The maximum values are reached at the end of the Q1 magnet for both cases.

Figure 4 shows a 2D map of $\mathcal{E}$ in the coils region superimposed to the transverse section of the magnet at the longitudinal position of the maximum. Because of the vertical crossing angle in the IP, the distribution displays the hottest spot on the upper pole.

[2]Previous calculations [5] assessed the quench limit to be 0.8 mJ/cm^3.

[3]This value is compatible with 1.6 mW/g [2].

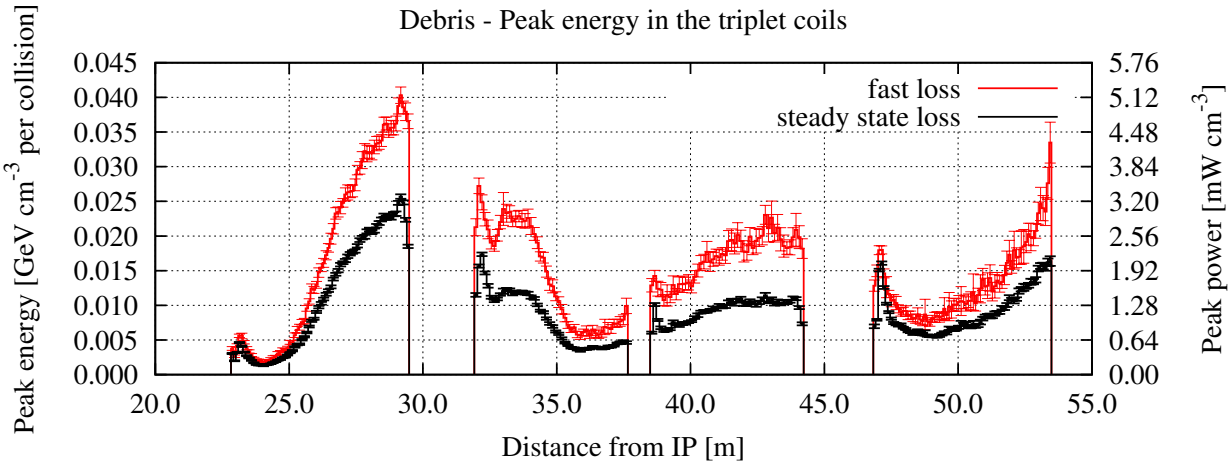

Figure 3: *Longitudinal profile of peak($\mathcal{E}$) and peak($\mathcal{E}_{cable}$) along the coils of the magnets of the inner triplet, induced by the proton-proton collision debris. The red curve shows the energy density calculated for fast losses (fine mesh, peak energy scale) and the black one for steady state losses at nominal luminosity (mesh corresponding to the cable size, peak power scale). Vertical bars indicate the statistical errors.*

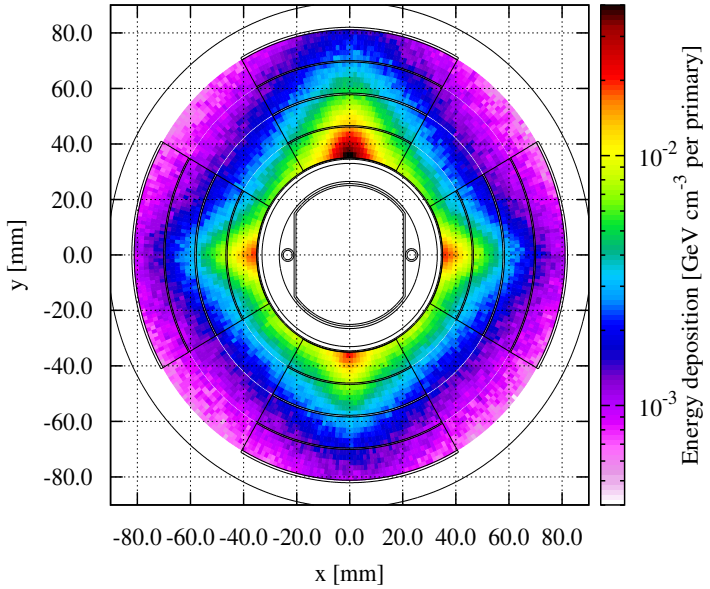

Figure 4: *2D map of the energy deposition in the Q1 magnet, at the longitudinal position of the maximum, due to the proton-proton collision debris.*

The longitudinal profiles of the peak values of $\mathcal{E}$ and $\mathcal{E}_{cable}$ are shown in Figures 5, 6 and 7 for the *TAS-H*, *TAS-V* and *Q2B* loss scenarios, respectively. The profiles due to losses on the TAS show maximum values in the Q1 magnet, while the *Q2B* loss scenario affects mainly the central part of the Q2B magnet, as expected. In this last case, max($\mathcal{E}$) is roughly 50 times larger than in case of losses on the TAS. A summary of maximum values of energy density deposition due to collision debris and each loss scenario is presented in Table 2.

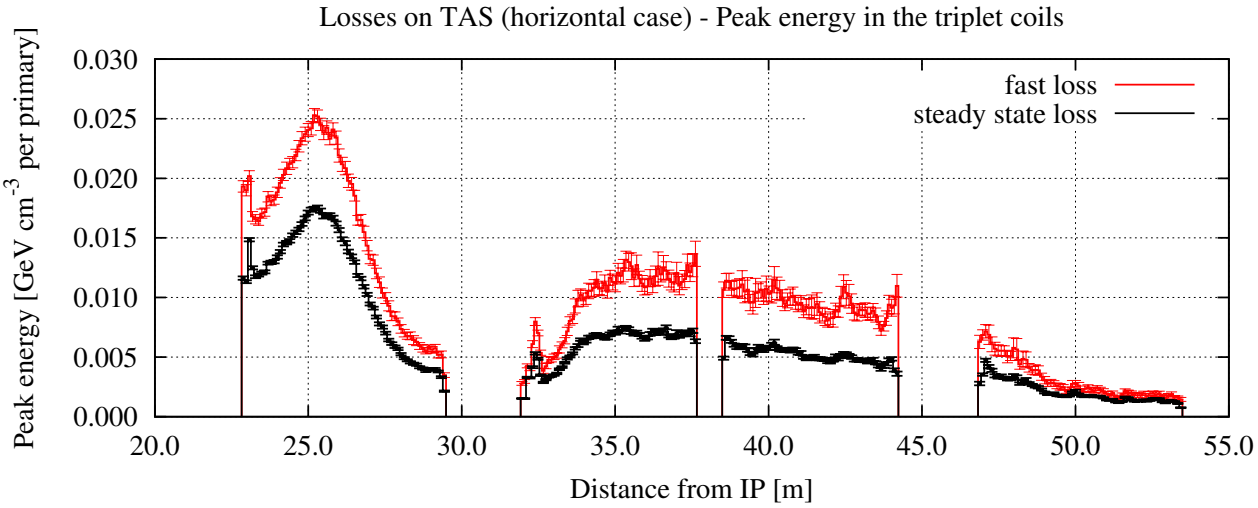

Figure 5: *Longitudinal profile of peak($\mathcal{E}$) (for fast transient losses, red curve) and peak($\mathcal{E}_{cable}$) (for steady state losses, black curve) along the magnets of the inner triplet in the TAS-H scenario. A primary event is the loss of a single proton. Vertical bars indicate the statistical errors.*

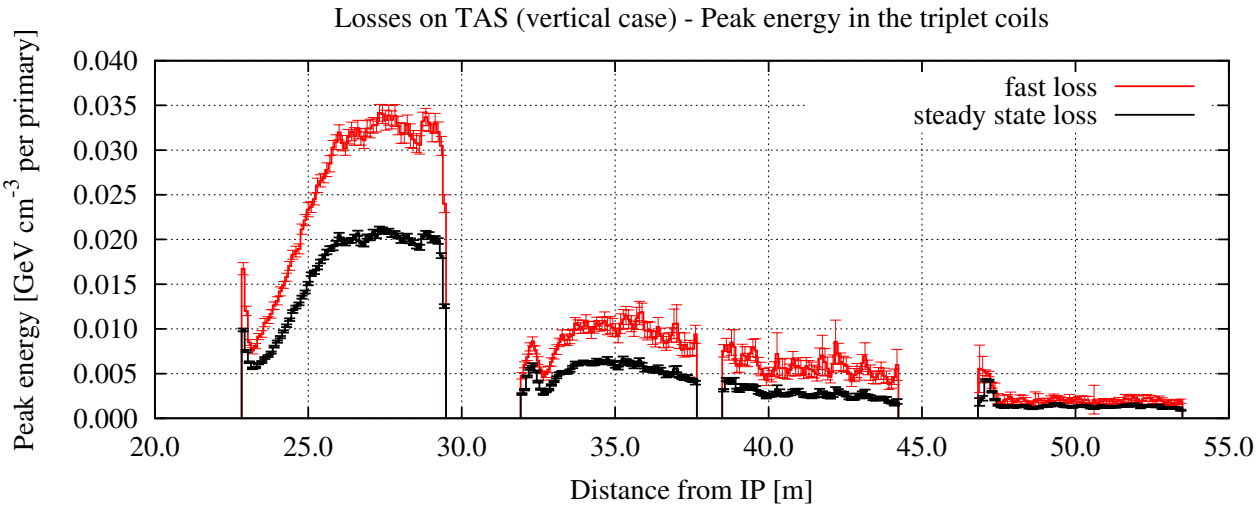

Figure 6: *The same as Figure 5 for the TAS-V scenario.*

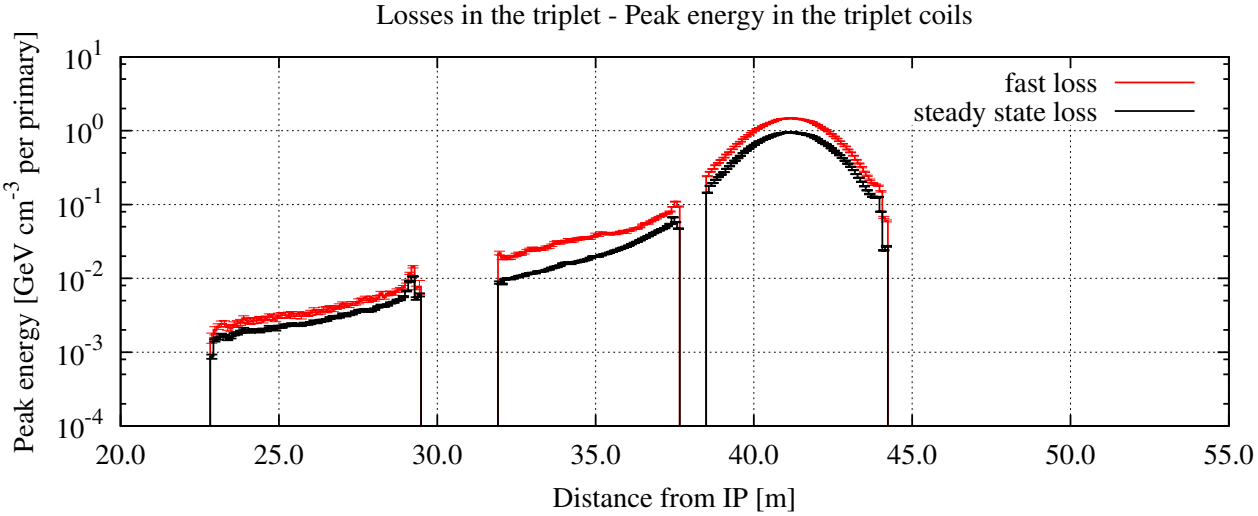

Figure 7: *The same as Figure 5 for the Q2B scenario. Values in Q3 coil are of the order of* 10^{-6} GeV/cm^3 *per primary.*

Table 2 also lists in the 5^{th} column the number of lost protons leading to quench in case of fast transient losses, calculated as:

$$\mathrm{N_{QL}} = \Delta \mathrm{H}/\max(\mathcal{E}) \tag{1}$$

and in the 8^{th} column the loss rate leading to quench in case of steady state losses, calculated as:

$$\mathrm{R_{QL}} = \mathcal{P}_{\mathrm{QL}}/\max(\mathcal{E}_{\mathrm{cable}}) \tag{2}$$

Equations 1 and 2 neglect the additional contemporary contribution of the collision debris to any of the abnormal losses. Apart from the fact that abnormal losses will likely depress this contribution, our final conclusions remain valid also if the latter is not negligible, as discussed later on.

For the *Q2B* scenario, the critical R_{QL} ($7.9{\cdot}10^7$ s^{-1}, see Table 2) is one order of magnitude lower if compared to the nominal collision rate ($8.0{\cdot}10^8$ s^{-1}, see Section 4.1). On the other hand, the critical N_{QL} ($5.1{\cdot}10^6$, see Table 2) is two orders of magnitude larger than the number of proton-proton collisions occurring in 40 μs (i.e. $3.2{\cdot}10^4$). This outcome already puts into context the challenge of effectively identifying such an abnormal loss scenario by the BLMs.

scenario	first magnet to quench	$\max(\mathcal{E})$ position [cm]	$\max(\mathcal{E})$ value [$\frac{\mathrm{GeV}}{\mathrm{cm}^3}$]	critical $\mathrm{N_{QL}}$	$\max(\mathcal{E}_{\mathrm{cable}})$ position [cm]	$\max(\mathcal{E}_{\mathrm{cable}})$ value [$\frac{\mathrm{GeV}}{\mathrm{cm}^3}$]	critical $\mathrm{R_{QL}}$ [s^{-1}]
debris	Q1	2917	0.040	-	2917	0.026	-
TAS-H	Q1	2503	0.026	$2.9 \cdot 10^8$	2539	0.018	$4.2 \cdot 10^9$
TAS-V	Q1	2818	0.034	$2.2 \cdot 10^8$	2800	0.022	$3.5 \cdot 10^9$
Q2B	Q2B	4114	1.48	$5.1 \cdot 10^6$	4114	0.948	$7.9 \cdot 10^7$

Table 2: *Maximum $\mathcal{E}$ and $\mathcal{E}_{cable}$ for the collision debris and for the beam loss scenarios considered in the present study. The first magnet to quench, the location of quench and the number of lost protons ($\mathrm{N_{QL}}$, for fast transient losses) and loss rate ($\mathrm{R_{QL}}$, for steady state losses) required to quench are indicated as well. In case of debris, the proton-proton collision rate that is predicted to lead to quench is a factor of a few higher than the one corresponding to nominal luminosity.*

7 Signals in the BLMs

A total of 18 BLMs are installed in the region of the *inner triplet* (see Section 2): Table 3 lists their longitudinal position and the value of the energy deposition in the *active* gas region per primary event. The contribution of the peripheral gas volume still affected by the presence of the electrodes was neglected. Signals in the BLMs are preferably expressed as dose, thus as ratio of the calculated energy deposition values to the respective gas mass (i.e. 2 g):

$$\mathrm{D_{BLM}[Gy]} = \frac{\mathrm{E_{BLM}[J]}}{\mathrm{m_{N_2}[kg]}} \tag{3}$$

Figure 8 shows typical fluence spectra of particles in a BLM: as can be seen, neutrons and photons are the most abundant species.

BLM No	z (dcum) [cm]	protected magnet /beam	debris		signal per lost proton E_{BLM} [10^{-6}GeV]		
			E_{pp} per coll. [10^{-6}GeV]	$\mathcal{D}_{pp}$ [Gy/s]	*TAS-H*	*TAS-V*	*Q2B*
1	2160	Q1/B2	10.8	$6.90 \cdot 10^{-4}$	1.39	1.11	-
2	2344	Q1/B1	2.53	$1.62 \cdot 10^{-4}$	2.95	2.37	0.35
3	2565	Q1/B2	1.17	$7.46 \cdot 10^{-5}$	1.04	1.14	0.74
4	2665	Q1/B1	1.61	$1.03 \cdot 10^{-4}$	1.29	1.08	0.89
5	2975	Q2A/B2	4.38	$2.80 \cdot 10^{-4}$	0.66	1.55	13.2
6	3230	Q1/B1	18.2	$1.17 \cdot 10^{-3}$	2.98	6.81	4.18
7	3412	Q2A/B2	4.42	$2.83 \cdot 10^{-4}$	1.56	1.56	5.66
8	3530	Q2A/B1	2.15	$1.37 \cdot 10^{-4}$	0.58	0.72	9.82
9	3741	Q2A/B2	1.36	$8.73 \cdot 10^{-5}$	0.75	0.50	28.6
10	3857	Q2B/B1	2.23	$1.43 \cdot 10^{-4}$	0.92	0.51	33.9
11	4081	Q2B/B2	1.36	$8.72 \cdot 10^{-5}$	0.54	0.23	60.2
12	4181	Q2B/B1	1.78	$1.14 \cdot 10^{-4}$	0.36	0.19	23.1
13	4362	Q3/B2	1.60	$1.02 \cdot 10^{-4}$	0.38	0.14	7.19
14	4669	Q2B/B1	10.4	$6.64 \cdot 10^{-4}$	1.15	0.82	1.28
15	4965	Q3/B2	1.24	$7.94 \cdot 10^{-5}$	0.22	0.18	0.55
16	5065	Q3/B1	1.03	$6.59 \cdot 10^{-5}$	0.16	0.10	0.45
17	5363	Q3/B2	1.43	$9.17 \cdot 10^{-5}$	0.09	0.12	0.30
18	5900	Q3/B1	71.3	$4.56 \cdot 10^{-3}$	4.12	3.46	0.13

Table 3: *Summary of simulated signals in the BLMs, for the collision debris and each loss scenario considered in this study. The fifth column is normalized to the nominal collision rate of* $8 \cdot 10^8$ s^{-1}.

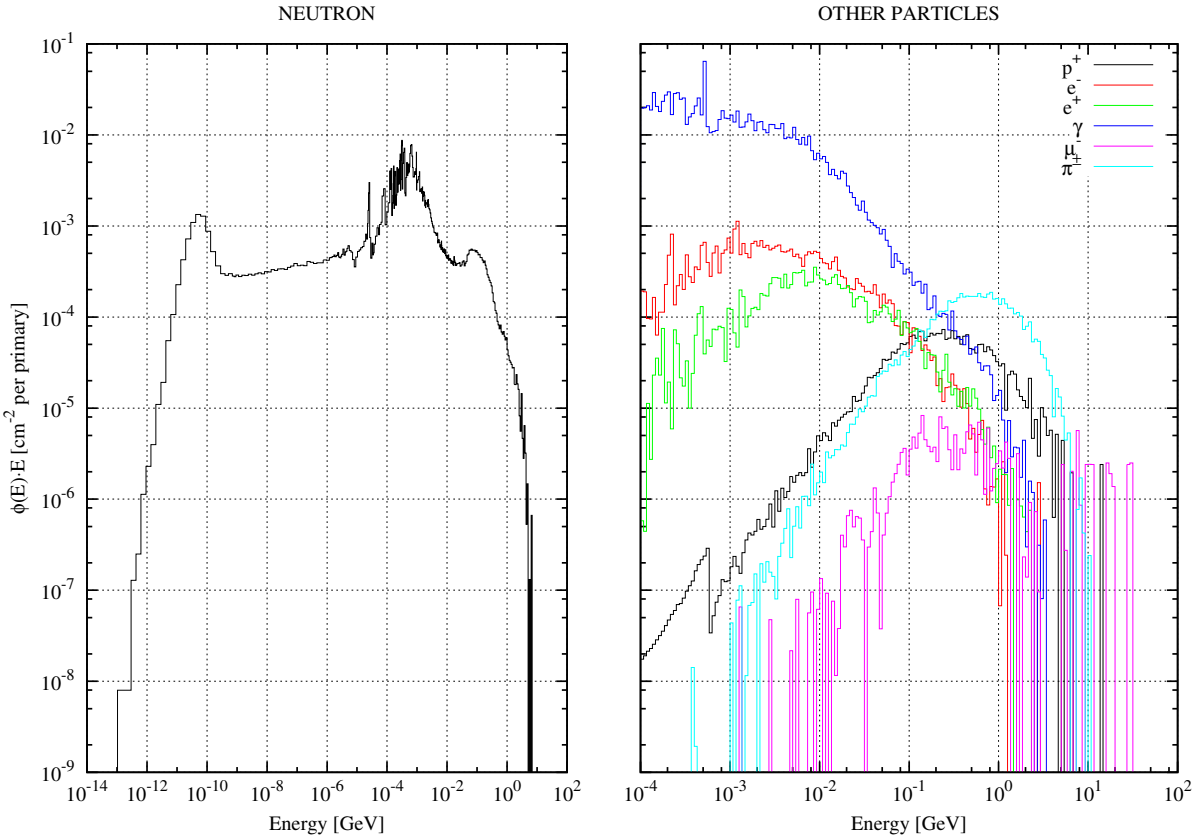

Figure 8: *Example of fluence spectra of particles in a BLM: neutron on the left frame, other relevant particle families on the right one. Note the different range of the x-axis. The considered BLM is the number 6, in the proton-proton collision scenario.*

7.1 Debris from IP

During stable collisions, each BLM signal due to the debris linearly scales with the actual luminosity. The calculated signals are shown in Figure 9, both as energy deposited in the BLMs per proton-proton collision (E_{pp}) and dose rate ($\mathcal{D}_{pp}$). The values are listed in columns 4 and 5 of Table 3.

The last BLM reads the highest value of 4.56 mGy/s, quite distinct if compared to the other BLMs, due to its favourable position, only 17 cm away from the center of the beam pipe. For a similar reason a high signal is read from the first monitor. BLMs number 6 and 14 read large values as well, because they are located downstream an interconnection between magnets, thus with quite less shielding by the cold mass.

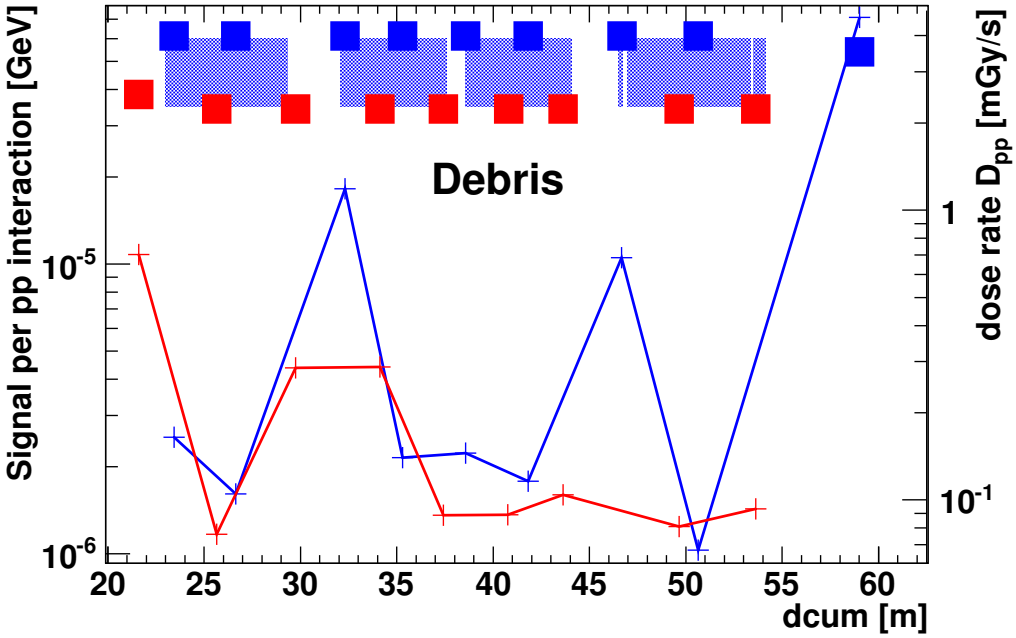

Figure 9: *Signals in the BLMs due to the collision debris, calculated as energy deposition in the active gas per proton-proton collision and scaled to nominal luminosity.*

7.2 Beam Losses on TAS and on Q2B

The values of the signals per proton lost on TAS or Q2B are listed in columns 6 through 8 of Table 3. The scenarios of losses on TAS (horizontal and vertical) give a similar pattern, with the highest responses at the beginning of Q1 and Q2A magnets and then at the BLM number 18.

In the case of the *Q2B* scenario, the pattern of the BLMs signal is obviously quite different, with strong responses in the BLMs just downstream the loss location (from number 12 to 9), and reduced values outside of this area, with a local peak in the BLM number 5, at the end of the "long" interconnection between Q2A and Q1. BLM 1 was not implemeted in the *Q2B* loss simulation, but is not expected to read a significant signal.

8 Proposals of Quench-Preventing Thresholds

Thresholds on BLMs signals should allow the safe and reliable operation of the machine, i.e. they should prevent magnet quench as well as avoid unnecessary beam dumps.

8.1 Fast Losses

The shortest integration time of the BLMs electronics is 40 μs: during such a short time the maximum energy density released by the debris in the coil is estimated at 0.2 μJ/cm^3, about 6000 times smaller than the enthalpy limit of the dry cable (ΔH). Therefore, for losses on this timescale the contribution from the debris can be neglected.

The signal at magnet quench, expressed as dose rate, is obtained by multiplying the BLM signal for a single proton (D_{BLM}) by the number of lost protons inducing the quench (N_{QL}) and dividing it by the shortest integration time of the system (40 μs) considered. Table 4 (columns 2, 4, 6) lists the BLM signals thus obtained for each loss scenario. The ratio of the signal from quenching losses to the signal generated by the debris is listed in columns 3, 5 and 7. The longitudinal pattern of the BLM signals is shown in Figure 10.

BLM	*TAS-H*		*TAS-V*		*Q2B*	
No	$\mathcal{D}_{QL}$ [Gy/s]	$\mathcal{D}_{QL}/\mathcal{D}_{pp}$	$\mathcal{D}_{QL}$ [Gy/s]	$\mathcal{D}_{QL}/\mathcal{D}_{pp}$	$\mathcal{D}_{QL}$ [Gy/s]	$\mathcal{D}_{QL}/\mathcal{D}_{pp}$
1	$8.07 \cdot 10^{-1}$	$1.2 \cdot 10^{3}$	$4.81 \cdot 10^{-1}$	$7.0 \cdot 10^{2}$	-	-
2	$1.71 \cdot 10^{0}$	$1.1 \cdot 10^{4}$	$1.03 \cdot 10^{0}$	$6.4 \cdot 10^{3}$	$3.54 \cdot 10^{-3}$	$2.2 \cdot 10^{1}$
3	$6.02 \cdot 10^{-1}$	$8.1 \cdot 10^{3}$	$4.97 \cdot 10^{-1}$	$6.7 \cdot 10^{3}$	$7.44 \cdot 10^{-3}$	$1.0 \cdot 10^{2}$
4	$7.47 \cdot 10^{-1}$	$7.3 \cdot 10^{3}$	$4.71 \cdot 10^{-1}$	$4.6 \cdot 10^{3}$	$9.04 \cdot 10^{-3}$	$8.8 \cdot 10^{1}$
5	$3.80 \cdot 10^{-1}$	$1.4 \cdot 10^{3}$	$6.72 \cdot 10^{-1}$	$2.4 \cdot 10^{3}$	$1.33 \cdot 10^{-1}$	$4.7 \cdot 10^{2}$
6	$1.73 \cdot 10^{0}$	$1.5 \cdot 10^{3}$	$2.96 \cdot 10^{0}$	$2.5 \cdot 10^{3}$	$4.23 \cdot 10^{-2}$	$3.6 \cdot 10^{1}$
7	$9.03 \cdot 10^{-1}$	$3.2 \cdot 10^{3}$	$6.78 \cdot 10^{-1}$	$2.4 \cdot 10^{3}$	$5.74 \cdot 10^{-2}$	$2.0 \cdot 10^{2}$
8	$3.35 \cdot 10^{-1}$	$2.4 \cdot 10^{3}$	$3.13 \cdot 10^{-1}$	$2.3 \cdot 10^{3}$	$9.94 \cdot 10^{-2}$	$7.2 \cdot 10^{2}$
9	$4.33 \cdot 10^{-1}$	$5.0 \cdot 10^{3}$	$2.16 \cdot 10^{-1}$	$2.5 \cdot 10^{3}$	$2.90 \cdot 10^{-1}$	$3.3 \cdot 10^{3}$
10	$5.35 \cdot 10^{-1}$	$3.7 \cdot 10^{3}$	$2.20 \cdot 10^{-1}$	$1.5 \cdot 10^{3}$	$3.44 \cdot 10^{-1}$	$2.4 \cdot 10^{3}$
11	$3.13 \cdot 10^{-1}$	$3.6 \cdot 10^{3}$	$1.00 \cdot 10^{-1}$	$1.1 \cdot 10^{3}$	$6.10 \cdot 10^{-1}$	$7.0 \cdot 10^{3}$
12	$2.08 \cdot 10^{-1}$	$1.8 \cdot 10^{3}$	$8.14 \cdot 10^{-2}$	$7.1 \cdot 10^{2}$	$2.34 \cdot 10^{-1}$	$2.0 \cdot 10^{3}$
13	$2.18 \cdot 10^{-1}$	$2.1 \cdot 10^{3}$	$6.06 \cdot 10^{-2}$	$5.9 \cdot 10^{2}$	$7.28 \cdot 10^{-2}$	$7.1 \cdot 10^{2}$
14	$6.66 \cdot 10^{-1}$	$1.0 \cdot 10^{3}$	$3.57 \cdot 10^{-1}$	$5.4 \cdot 10^{2}$	$1.29 \cdot 10^{-2}$	$1.9 \cdot 10^{1}$
15	$1.29 \cdot 10^{-1}$	$1.6 \cdot 10^{3}$	$7.76 \cdot 10^{-2}$	$9.8 \cdot 10^{2}$	$5.60 \cdot 10^{-3}$	$7.1 \cdot 10^{1}$
16	$9.10 \cdot 10^{-2}$	$1.4 \cdot 10^{3}$	$4.57 \cdot 10^{-2}$	$6.9 \cdot 10^{2}$	$4.51 \cdot 10^{-3}$	$6.8 \cdot 10^{1}$
17	$5.32 \cdot 10^{-2}$	$5.8 \cdot 10^{2}$	$5.04 \cdot 10^{-2}$	$5.5 \cdot 10^{2}$	$3.06 \cdot 10^{-3}$	$3.3 \cdot 10^{1}$
18	$2.39 \cdot 10^{0}$	$5.2 \cdot 10^{2}$	$1.51 \cdot 10^{0}$	$3.3 \cdot 10^{2}$	$1.31 \cdot 10^{-3}$	$2.9 \cdot 10^{-1}$

Table 4: *Values of the signal in the BLMs at magnet quench for different scenarios of* 40 μs *long losses (columns 2, 4 and 6) and ratios to the signal from debris (columns 3, 5 and 7).*

From Table 4 and Figure 10, one can realize that also the signal in the BLMs is dominated by the losses, with a negligible contribution from the debris: even though the signals per primary event in each considered scenario are roughly of the same order of magnitude (as in Table 3), values of N_{QL} (see Table 2) are by far larger than the number of collisions occurring in 40 μs, as already mentioned at the end of Section 6.

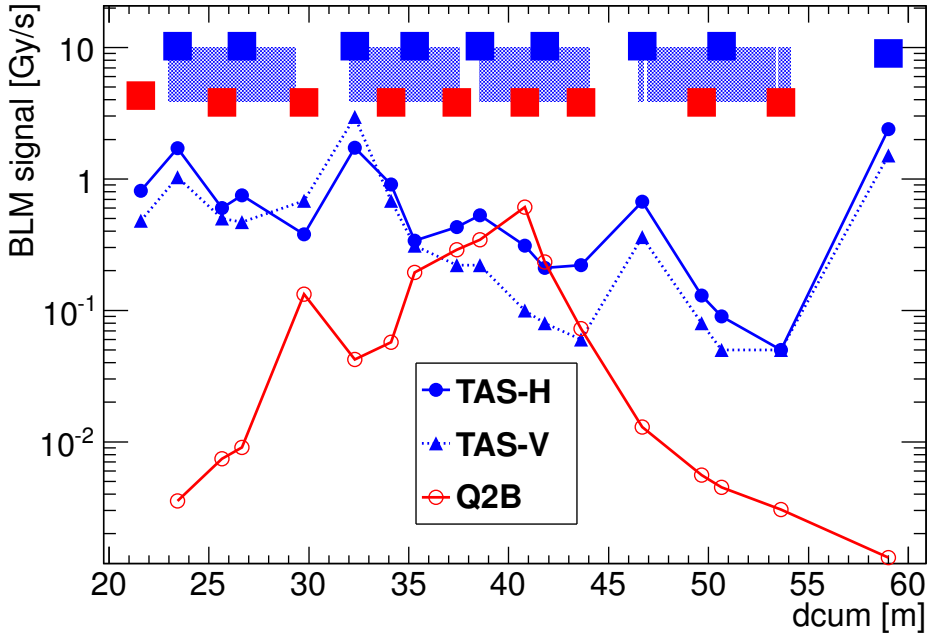

Figure 10: *Signals in the BLMs at magnet quench for the three considered scenarios of proton fast losses. The signal from the collision debris reported in Figure 9 is below the lower scale limit.*

The *Q2B* loss scenario shows the lowest signal at quench for the most sensitive BLM: losses take place inside the Q2B magnet, impacting more directly the coils and displaying a larger energy deposition gradient between coils and BLMs. The BLM peak signal is 0.61 Gy/s: a typical 30% fraction of this value could be recommended as sensible threshold for preventing quench, therefore a value of 0.2 Gy/s is proposed. This threshold is crossed by 15 monitors in case of *TAS-H* losses, 12 monitors in case of *TAS-V* losses and 4 monitors in case of localized *Q2B* losses. For comparison the estimated threshold for the main dipoles of LHC is 0.18 Gy/s [24] for 7 TeV beam energy and the same integration time.

8.2 Steady State Losses

In case of steady state losses the deposited heat is constantly evacuated through the cooling system of the magnet: the equilibrium between heat deposition and removal is achieved on a timescale of the order of seconds.

The reported scenario considers that, as the loss develops, the collision rate diminishes and becomes negligible. Therefore no debris is longer present and only beam losses induce coil heating as well as the BLM signal. The opposite extreme case where the loss development does not affect the proton-proton collision rate has been investigated as well, and the final conclusions are similar.

The BLM dose rate at magnet quench is obtained by multiplying the BLM signal per single proton (D_{BLM}) by the rate of lost protons inducing the quench (R_{QL}). Table 5 (columns 2, 4, 6) lists the BLM signals thus obtained for each loss scenario. Their ratios to the signal generated by the debris are listed in columns 3, 5 and 7. The longitudinal pattern of the BLM signals is shown in Figure 11.

Contrary to what happens in case of fast losses, Table 5 and Figure 11 show that the signals in the BLMs due to any beam loss scenario cannot be clearly distinguished from the signals due to the collision debris: in this case the values of R_{QL} (see Table 2) are not so higher (*TAS*) or even quite lower (*Q2B*) with respect to the rate of collisions, and the assessment of thresholds becomes impracticable.

BLM	*TAS-H*		*TAS-V*		*Q2B*	
No	$\mathcal{D}_{\mathrm{QL}}$ [Gy/s]	$\mathcal{D}_{\mathrm{QL}}/\mathcal{D}_{\mathrm{pp}}$	$\mathcal{D}_{\mathrm{QL}}$ [Gy/s]	$\mathcal{D}_{\mathrm{QL}}/\mathcal{D}_{\mathrm{pp}}$	$\mathcal{D}_{\mathrm{QL}}$ [Gy/s]	$\mathcal{D}_{\mathrm{QL}}/\mathcal{D}_{\mathrm{pp}}$
1	$4.64 \cdot 10^{-4}$	$6.7 \cdot 10^{-1}$	$3.07 \cdot 10^{-4}$	$4.5 \cdot 10^{-1}$	-	-
2	$9.83 \cdot 10^{-4}$	$6.1 \cdot 10^{0}$	$6.60 \cdot 10^{-4}$	$4.1 \cdot 10^{0}$	$2.21 \cdot 10^{-6}$	$1.4 \cdot 10^{-2}$
3	$3.46 \cdot 10^{-4}$	$4.6 \cdot 10^{0}$	$3.17 \cdot 10^{-4}$	$4.3 \cdot 10^{0}$	$4.65 \cdot 10^{-6}$	$6.2 \cdot 10^{-2}$
4	$4.29 \cdot 10^{-4}$	$4.2 \cdot 10^{0}$	$3.01 \cdot 10^{-4}$	$2.9 \cdot 10^{0}$	$5.65 \cdot 10^{-6}$	$5.5 \cdot 10^{-2}$
5	$2.18 \cdot 10^{-4}$	$7.8 \cdot 10^{-1}$	$4.29 \cdot 10^{-4}$	$1.5 \cdot 10^{0}$	$8.33 \cdot 10^{-5}$	$3.0 \cdot 10^{-1}$
6	$9.94 \cdot 10^{-4}$	$8.5 \cdot 10^{-1}$	$1.89 \cdot 10^{-3}$	$1.6 \cdot 10^{0}$	$2.65 \cdot 10^{-5}$	$2.3 \cdot 10^{-2}$
7	$5.19 \cdot 10^{-4}$	$1.8 \cdot 10^{0}$	$4.33 \cdot 10^{-4}$	$1.5 \cdot 10^{0}$	$3.59 \cdot 10^{-5}$	$1.3 \cdot 10^{-1}$
8	$1.92 \cdot 10^{-4}$	$1.4 \cdot 10^{0}$	$2.00 \cdot 10^{-4}$	$1.5 \cdot 10^{0}$	$6.22 \cdot 10^{-5}$	$4.5 \cdot 10^{-1}$
9	$2.49 \cdot 10^{-4}$	$2.8 \cdot 10^{0}$	$1.38 \cdot 10^{-4}$	$1.6 \cdot 10^{0}$	$1.81 \cdot 10^{-4}$	$2.1 \cdot 10^{0}$
10	$3.08 \cdot 10^{-4}$	$2.2 \cdot 10^{0}$	$1.40 \cdot 10^{-4}$	$9.8 \cdot 10^{-1}$	$2.15 \cdot 10^{-4}$	$1.5 \cdot 10^{0}$
11	$1.80 \cdot 10^{-4}$	$2.1 \cdot 10^{0}$	$6.39 \cdot 10^{-5}$	$7.3 \cdot 10^{-1}$	$3.81 \cdot 10^{-4}$	$4.4 \cdot 10^{0}$
12	$1.20 \cdot 10^{-4}$	$1.1 \cdot 10^{0}$	$5.20 \cdot 10^{-5}$	$4.6 \cdot 10^{-1}$	$1.46 \cdot 10^{-4}$	$1.3 \cdot 10^{0}$
13	$1.25 \cdot 10^{-4}$	$1.2 \cdot 10^{0}$	$3.87 \cdot 10^{-5}$	$3.8 \cdot 10^{-1}$	$4.55 \cdot 10^{-5}$	$4.5 \cdot 10^{-1}$
14	$3.83 \cdot 10^{-4}$	$5.8 \cdot 10^{-1}$	$2.28 \cdot 10^{-4}$	$3.4 \cdot 10^{-1}$	$8.08 \cdot 10^{-6}$	$1.2 \cdot 10^{-2}$
15	$7.39 \cdot 10^{-5}$	$9.3 \cdot 10^{-1}$	$4.95 \cdot 10^{-5}$	$6.2 \cdot 10^{-1}$	$3.50 \cdot 10^{-6}$	$4.4 \cdot 10^{-2}$
16	$5.23 \cdot 10^{-5}$	$7.9 \cdot 10^{-1}$	$2.91 \cdot 10^{-5}$	$4.4 \cdot 10^{-1}$	$2.82 \cdot 10^{-6}$	$4.3 \cdot 10^{-2}$
17	$3.06 \cdot 10^{-5}$	$3.3 \cdot 10^{-1}$	$3.22 \cdot 10^{-5}$	$3.5 \cdot 10^{-1}$	$1.92 \cdot 10^{-6}$	$2.1 \cdot 10^{-2}$
18	$1.37 \cdot 10^{-3}$	$3.0 \cdot 10^{-1}$	$9.62 \cdot 10^{-4}$	$2.1 \cdot 10^{-1}$	$8.19 \cdot 10^{-7}$	$1.8 \cdot 10^{-4}$

Table 5: *Values of the signal in the BLMs at magnet quench for different scenarios of steady state losses (columns 2, 4 and 6) and ratios to the signal from debris (columns 3, 5 and 7).*

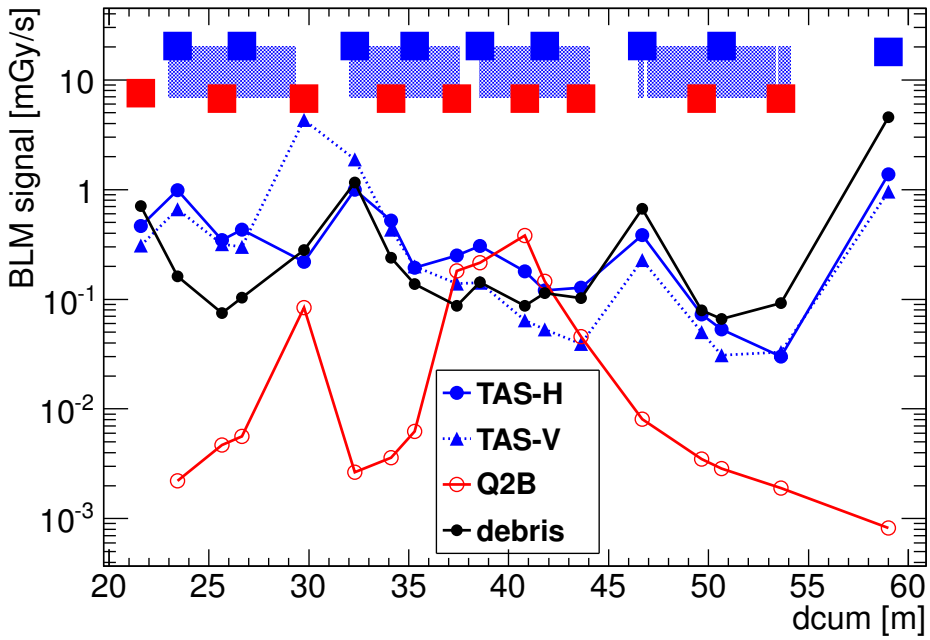

Figure 11: *BLM signals due to collision debris (black curve), and BLM signals at magnet quench for the three considered scenarios of proton steady state losses.*

For example, in the case of *Q2B* beam losses, most of the triplet BLMs get actually a lower response than the one due to the collision debris. The highest signal, read by the BLM number 11, is about 400 μGy/s. The typical 30% fraction of this value could be recommended as threshold, but that turns out to be quite close to the debris signal of $\sim$ 90 μGy/s, possibly interfering with the normal operation in stable collisions conditions at nominal luminosity.

8.3 Estimation of Errors

Results from Monte Carlo calculations like those presented here are affected by unavoidable sources of systematic uncertainties mainly related to:

- geometry and material implementation. In particular, many ancillary beam line elements (like flanges, valves...) not included at the stage of this work can affect the estimation of the BLM responses. Thus, the collection of numbers here reported as a support for our conclusions is not intended to be taken literally;
- strong dependence on a very small angular range of the reaction products;
- extrapolation of the cross sections for the primary events;
- interaction modeling.

These uncertainties are particularly important in case of steady state losses because the BLM signals corresponding to a loss induced quench are close to the one from the collision debris.

9 Conclusions

The aim of the present study is to investigate the possibility of assessing thresholds in the BLM system in order to protect the magnets of the *inner triplet* from quench induced by abnormal losses. Three loss scenarios are considered, two of which deal with the geometrical aperture limitation at the TAS (*TAS-H* and *TAS-V*); the third one (*Q2B*) refers to wrong settings of the collimators.

For **fast transient losses** (over 40 μs) the BLMs placed close to the loss location would be able to prevent the magnets from quenching and a conservative threshold value is 0.2 Gy/s. This can be compared to that used at Tevatron at beam energy of 1 TeV [25], which is about 70 μGy, i.e. 1.75 Gy/s for 40 μs fast losses, and to the one of the main dipoles of LHC at 7 TeV beam energy, which is 0.18 Gy/s [24].

In case of **steady-state losses** the situation is more complicated as the signals from quench inducing losses do not stand out against those produced by the collision debris. A long-term solution to this problem should be studied. A few approaches are possible, for instance:

- a "topological threshold", for which the beam dump signal is triggered when the longitudinal profile of the measured dose changes in shape;
- the use of thermometers detecting the critical coil temperature - this is a feasible solution since the interference with the debris contribution shows up only for relatively long losses;
- the installation of detectors close to the coils, so that the measured dose is more directly linked to the dose actually received by the coils.

These strategies might be particularly important for the upgrade of the LHC towards higher values of luminosity.

References

[1] "LHC Design Report, Vol. I The LHC main ring", CERN-2004-003, June 2004;

[2] N.V. Mokhov, I.L. Rakhno, J.S. Kerby, J.B. Strait, "Protecting LHC IP1/IP5 Components Against Radiation Resulting from Colliding Beam Interactions", LHC Project Report 633, 2003;

[3] for an overview of the LHC BLM system see `http://cern.ch/blm`;

[4] M. Stockner, "Beam Loss Calibration Studies for High Energy Proton Accelerators", PhD thesis, CERN 2007;

[5] J.B. Jeanneret, D. Leroy, L. Oberli, T. Trenkler, "Quench Levels and Transient Beam Losses in LHC Magnets", LHC Project Report 044, 1996;

[6] A. Fassò, A. Ferrari, J. Ranft, P.R. Sala, "FLUKA: a Multi-Particle Transport Code", CERN-2005-10, INFN/TC-05/11, SLAC-R-773;

[7] G. Battistoni, S. Muraro, P.R. Sala, F. Cerutti, A. Ferrari, S. Roesler, A. Fassò, J. Ranft, "The FLUKA code: Description and Benchmarking", proceedings of the Hadronic Shower Simulation Workshop 2006, Fermilab 6^{th}–8^{th} September 2006, M. Albrow, R. Raja eds., AIP Conference Proceeding 896, 31-49, 2007;

[8] C. Hoa, F. Cerutti, E. Wildner, "Energy Deposition in the LHC Insertion Regions IR1 and IR5", LHC Project Note 1167, 2008;

[9] A. Mereghetti, "Update on Radiation Levels in IR1 and IR5", presentation at the Radiation To Electronics Study Group, April 29^{th}, 2009;

[10] L. Sarchiapone et al.,"FLUKA Monte Carlo Simulations and Benchmark Measurements for the LHC Beam Loss Monitor", Nucl. Instr. and Meth. A, Vol 581, Issues 1-2, pages 511-516, 2007;

[11] N.V. Mokhov, "Tertiary Collimators in IP1/IP5 Progress Report", presentation at CERN/LARP Collimation Meeting, August 23^{rd}, 2006;

[12] S. Roesler, R. Engel, J. Ranft, "The Monte Carlo Event Generator DPMJET-III", Proceedings of the Monte Carlo 2000 Conference, Lisbon, October 23^{rd}–26^{th} 2000, Springer-Verlag Berlin, 1033-1038, 2001;

[13] C. Bracco, private communication;

[14] T. Weiler, private communication;

[15] "ROXIE: Routine for the Optimization of Magnet X-Sections, Inverse Field Calculation and Coil End Design", Proceedings of the 1^{st} International Roxie Users Meeting and Workshop, CERN, Geneva, March 16^{th}–18^{th} 1998, S. Russenschuck eds., CERN yellow report 99-01, 1999;

[16] L. Burnod, et al., "Thermal Modelling of the LHC Dipoles Functioning in Superfluid Helium", Proc. 4^{th} European Part. Accel. Conf., London, England, 1994;

[17] R. Bossert, et al., "Development of a High Gradient Quadrupole for the LHC Interaction Regions", IEEE Trans. Appl. Superconductivity 7, 1997;

[18] A.V. Zlobin, E. Barzi, D. Chichili et al., "Large-Aperture Nb_3Sn Quadrupoles for 2^{nd} Generation LHC IRs", Proc. of the European Part. Accel. Conf., Paris, June 3^{rd}–7^{th}, 2002, pp. 2451-2453; `http://accelconf.web.cern.ch/accelconf/e02/PAPERS/MOPLE017.pdf`.

[19] Seog-Whan Kim, "Quench Simulation of Multi-Strand Cable by an Equivalent Circuit", Fermilab TD-00-022, 2000;

[20] D. Bocian, B. Dehning, A. Siemko, "Modelling of Quench Limit for Steady State Heat Deposits in LHC Magnets", IEEE Trans. Appl. Superconductivity 19, 2009;

[21] P.P. Granieri, M. Calvi, A. Siemko, P. Xydi, "Modeling of Cable Stability Margin for Transient Perturbations", presentation at the THERMOMAG-07 conference, Paris, November 19^{th}–20^{th} 2007;

[22] A. Verweij, "QP3 User Manual", report in publication;

[23] F. Borgnolutti et al., "Energy Deposition in the LHC High Luminosity Insertions", proceedings of HHH-2008, W. Scandale and F. Zimmermann eds., CERN-2009-004, 2009;

[24] M. Sapinski, B. Dehning, A. Priebe, "Simulation of Beam Loss in LHC MB Magnet and Quench Threshold Test", LHC Project Note 422, 2009;

[25] D. Still, "Collimation Experience at the Tevatron", presentation at Collimation WG, CERN, April 15^{th}, 2005;